

Empirical evidence of an energy dependence of the radial shape of the real part of the optical potential

C. Mahaux and R. Sartor

Institut de Physique B5, Université de Liège, B-4000 Liège 1, Belgium

(Received 8 April 1986)

From a compilation of the real parts of phenomenological optical-model potentials which yield very good fits to the differential cross sections, it is concluded that in the cases of protons and neutrons on ^{208}Pb and of protons on ^{40}Ca the radial shape of the potential varies rapidly with energy for bombarding energies smaller than 20 MeV. The potential half-depth radius decreases with increasing energy, while the surface diffuseness tends to increase with energy. This empirical energy dependence is stronger than the one calculated in the framework of a theoretical nuclear matter approach.

I. INTRODUCTION

Optical-model analyses of elastic scattering cross sections of neutrons by ^{208}Pb have recently indicated that, for this system, the radial shape of the real part $V(r;E)$ of the optical-model potential (OMP) depends upon the bombarding energy E in the domain $4 < E < 24$ MeV.¹⁻³ This finding is of much practical interest. Indeed, it raises a doubt concerning the reliability of the usual procedure for estimating cross sections at low energy by using an optical-model potential which has the same radial shape as that determined by fitting experimental cross sections at higher energy. It also raises a theoretical problem, since we shall see in Sec. VI that it is at variance with a theoretical model of much current use, which predicts a much weaker energy dependence. It is therefore of interest to investigate whether similar empirical evidence also exists for other systems. This is the main purpose of the present paper.

Very accurate fits to the experimental cross sections can practically always be obtained within the assumption that $V(r;E)$ has a Woods-Saxon shape, viz.,

$$V(r;E) = \frac{V_0}{1 + \exp[(r-R)/a]}, \quad (1)$$

$$R = r_0 A^{1/3}. \quad (2)$$

This implies that the experimental data typically can determine only two shape parameters, namely r_0 and a in the Woods-Saxon case. Furthermore, a separate determination of r_0 and a requires that very accurate optical-model fits be performed and, of course, that r_0 and a be both considered as adjustable parameters in the optimization of the fit. In order to exhibit any systematic energy dependence, such fits must, moreover, be available in a sizeable energy domain.

A careful search through the literature left us with only three systems for which these three requirements are fulfilled, namely protons on ^{208}Pb and ^{40}Ca and neutrons on ^{208}Pb . The corresponding reference sources are specified in Sec. II. Section III is devoted to the energy dependence of three radial moments of $V(r;E)$ and Sec. IV with the

corresponding moment ratios. These ratios are of interest because they are independent of the potential strength, and are therefore characteristic of the radial shape of $V(r;E)$. In Sec. V we argue that, within the assumption that $V(r;E)$ has a Woods-Saxon shape, these moment ratios are equivalent to the knowledge of the shape parameters r_0 and a . This is of interest because, from current theoretical nuclear matter approaches, one can directly determine radial moments and moment ratios rather than the shape parameters r_0 and a . In Sec. VI we show that the energy dependence of r_0 and a predicted by the nuclear matter approach of Ref. 4 is much weaker than that exhibited by our compilation of the empirical values. Section VII contains a summary and a discussion.

II. RETAINED EMPIRICAL POTENTIALS

Since we want to investigate whether compilations of empirical OMP's show evidence for an energy dependence of the geometrical parameters r_0 and a , we only retain optical-model analyses in which these two parameters are adjusted at each energy in order to optimize the fit to the experimental cross sections. Furthermore, we only retain those OMP's which yield "very good" fits to the differential cross sections, as appreciated by Perey and Perey⁵ for analyses prior to 1975 and by ourselves for analyses performed since then. It turns out that despite the very large number of published phenomenological optical-model analyses, we found only three systems for which "retainable" optical-model potentials exist in an energy domain sufficiently broad to enable one to draw reliable conclusions concerning a possible energy dependence of the radial shape of $V(r;E)$. These are the systems p- ^{208}Pb , n- ^{208}Pb , and p- ^{40}Ca . We now list the reference sources of these retained empirical potentials.

(a) *Protons on ^{208}Pb .* Empirical OMP's which satisfy the requested conditions are available in Ref. 6 ($E=16$ MeV), Ref. 7 ($E=16, 21, 24.1, 30.5, 30.8, 35,$ and 40 MeV), Ref. 8 ($E=30.3$ MeV), Ref. 9 ($E=30.3$ MeV), Ref. 10 (two OMP's at $E=30.3$ MeV), Ref. 11 (two OMP's at $E=30.3$ MeV, two OMP's at $E=40$ MeV), Ref. 12 ($E=40$ MeV), and Ref. 13 ($E=40$ MeV).

TABLE I. Coefficients of the quadratic least squares fits to $[r^q]$.

	q	A_q (MeV fm $^{q+1}$)	B_q (fm $^{q+1}$)	$10^2 C_q$ (MeV $^{-1}$ fm $^{q+1}$)
p- ^{208}Pb	0.8	-92.9	1.67	-2.00
	2	-792	21.5	-28.5
	4	-38 487	1381	1948
n- ^{208}Pb	0.8	-58.3	0.314	0.0219
	2	-425	4.13	-2.28
	4	-17 649	282.7	260.4
p- ^{40}Ca	0.8	-141	1.21	-0.402
	2	-515	1.43	5.23
	4	-6860	-118.1	317.9

(b) *Neutrons on ^{208}Pb .* The retained empirical OMP's are taken from Ref. 14 ($E=9, 11, \text{ and } 26$ MeV), Ref. 1 ($E=7, 9, 11, 20, 22, 24, 25.7, 30, \text{ and } 40$ MeV), Ref. 15 (four OMP's at $E=10$ MeV), and line IIIa in Table I of Ref. 2 ($E=4, 4.5, 5, 5.5, 6, 6.5, \text{ and } 7$ MeV). In the latter case, the seven OMP's share the same values of r_0 and a ; we nevertheless included them because the fits and the measurements are very accurate, while the energy domain is quite narrow.

(c) *Protons on ^{40}Ca .* The retained empirical OMP's are selected from Ref. 16 ($E=9.6, 12.44, 14.6, 17.3, \text{ and } 19.57$ MeV), Ref. 17 ($E=17.3, 21.05, 35.8, \text{ and } 40.0$ MeV), and Ref. 18 ($E=20.58, 21.05, \text{ and } 21.68$ MeV).

III. RADIAL MOMENTS

We define radial moments $[r^q]$ as follows:

$$[r^q(E)] = \frac{4\pi}{A} \int_0^\infty V(r; E) r^q dr. \quad (3)$$

The global strength of the OMP is usually characterized by the volume integral per nucleon, $[r^2]$. We showed recently¹⁹ that the moment $[r^{0.8}]$ is better determined than $[r^2]$ in the sense that, when plotted versus energy, the empirical values of $[r^{0.8}]$ show less scatter than those of $[r^2]$ about averages defined by least squares fits with polynomials of second or third order in E . The values of $[r^4]$ are of interest because the mean square radius is given by the ratio

$$\langle r^2 \rangle = [r^4] / [r^2]. \quad (4)$$

The values of $[r^{0.8}]$, $[r^2]$, and $[r^4]$ associated with the retained empirical OMP are represented by crosses in Figs. 1–3, in which the solid curves represent least squares fits with the parametric expression

$$[r^q(E)] = A_q + B_q E + C_q E^2. \quad (5)$$

The coefficients A_q , B_q , and C_q are listed in Table I.

In the case of protons on ^{208}Pb (Fig. 1) the empirical values show little scatter about the least squares fit; the scatter increases as the exponent q in the moment $[r^q]$ increases, in keeping with the results of Ref. 19. The same remarks apply to the system n- ^{208}Pb (Fig. 2). In the case

of protons on ^{40}Ca , the scatter of the empirical values is also quite small, except for one point at $E=17.3$ MeV; this point is associated with an OMP taken from Ref. 16; the corresponding χ^2 per data point is 3 times larger than in the case of the OMP obtained at the same energy in Ref. 17; the latter yields points located close to the least squares fits, as seen in Fig. 3.

The quadratic least squares fits, Eq. (5), yield the following approximation for the difference between the

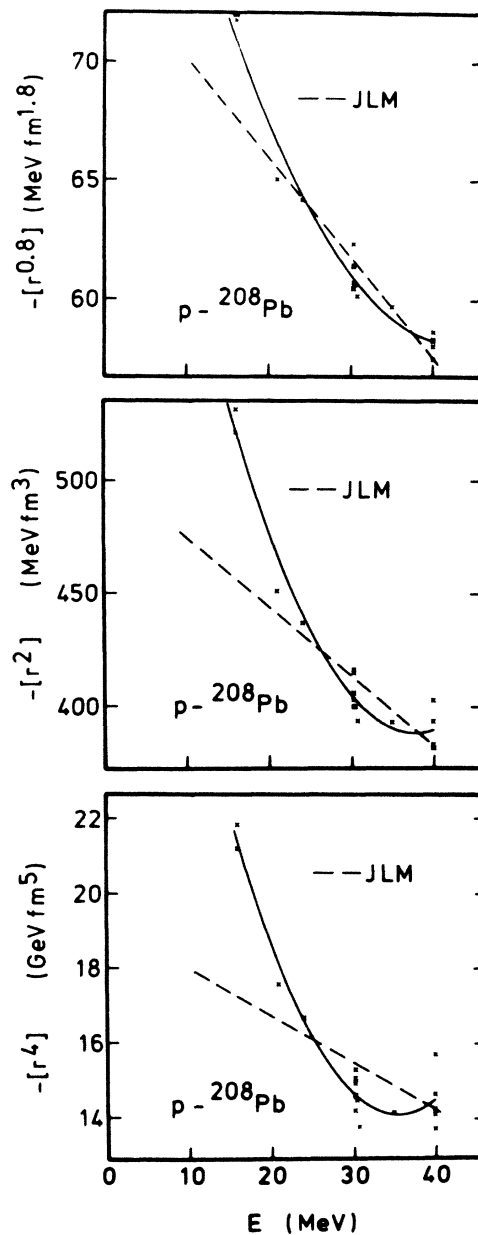


FIG. 1. The crosses represent the radial moments $[r^{0.8}]$ (in MeV fm $^{1.8}$), $[r^2]$ (in MeV fm 3), and $[r^4]$ (in GeV fm 5) associated with empirical OMP's for protons on ^{208}Pb (see Sec. II). The solid curves are quadratic least squares fits. The dashes have been calculated from the nuclear matter approach of Ref. 4.

volume integrals per nucleon for OMP's of, respectively, neutrons and protons on ^{208}Pb ($[r^2]$ in MeV fm^3 , E in MeV),

$$[r^2]^{(n)} - [r^2]^{(p)} = 367.6 - 17.36E + 0.262E^2, \quad (6a)$$

for energies contained in the domain $16 \leq E \leq 40$ MeV . The corresponding numerical value decreases from 125 MeV fm^3 at $E=20$ MeV to 92 MeV fm^3 at $E=40$ MeV . This result can be compared with a previous approximation by Rapaport,²⁰ who proposed

$$[r^2]^{(n)} - [r^2]^{(p)} = 98 - 0.45E; \quad (6b)$$

the latter approximation decreases from 89 MeV fm^3 at $E=20$ MeV to 80 MeV fm^3 at $E=40$ MeV . If the volume integral of the Coulomb correction, J_C/A , is set equal to 52 MeV fm^3 , as in Ref. 20, the volume integral per nucleon of the isovector component OMP is found to be equal to $J_1/A = 173 \text{ MeV fm}^3$ [Eq. (6a)] or 87 MeV fm^3 [Eq. (6b)] at $E=20$ MeV , while at $E=40$ MeV one obtains $J_1/A = 95 \text{ MeV fm}^3$ [Eq. (6a)] or 66 MeV fm^3 [Eq. (6b)]. We note, however, that at $E \approx 20$ MeV it appears more appropriate²¹ to take $J_C/A \approx 70 \text{ MeV fm}^3$, in which case Eq. (6a) yields $J_1/A \approx 130 \text{ MeV fm}^3$ at $E=20$ MeV .

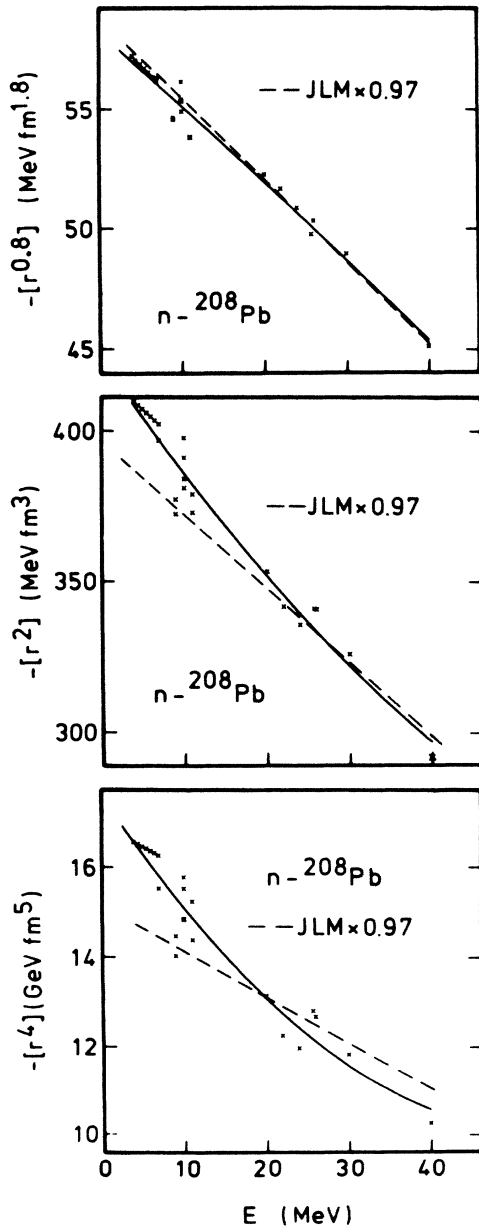


FIG. 2. Same as Fig. 1, in the case of neutrons on ^{208}Pb . The moments calculated from the nuclear matter approach have been multiplied by 0.97.

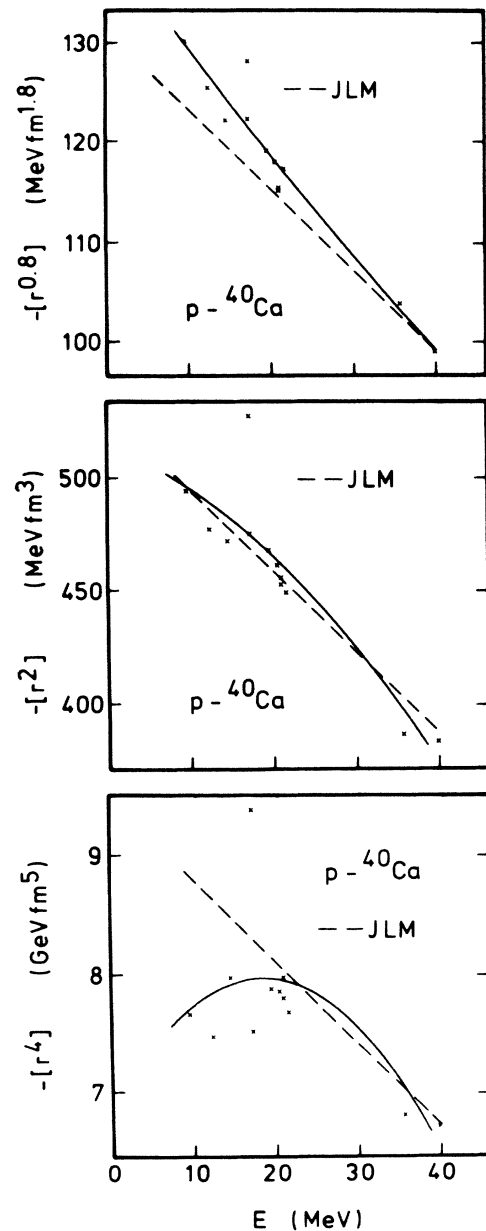


FIG. 3. Same as Fig. 1, in the case of protons on ^{40}Ca .

Our analysis therefore suggests the following approximation,

$$J_1/A \approx 165 - 1.75E, \quad (7)$$

for the volume integral per nucleon of the isovector component of the OMP in the domain $20 \leq E \leq 40$ MeV.

IV. RATIOS OF RADIAL MOMENTS

If the radial shape of the OMP would be independent of energy, the ratio $[r^q]/[r^{q'}]$ of two different radial moments would be independent of energy. Conversely, the radial shape depends upon energy if one ratio $[r^q]/[r^{q'}]$ varies with energy. It is therefore of interest to consider the quantity

$$T_{q/q'} = \{[r^q]/[r^{q'}]\}^{1/(q-q')}; \quad (8)$$

an exponent $(q-q')^{-1}$ has been introduced so that $T_{q/q'}$ has the dimension of a length. The familiar root mean square radius is given by

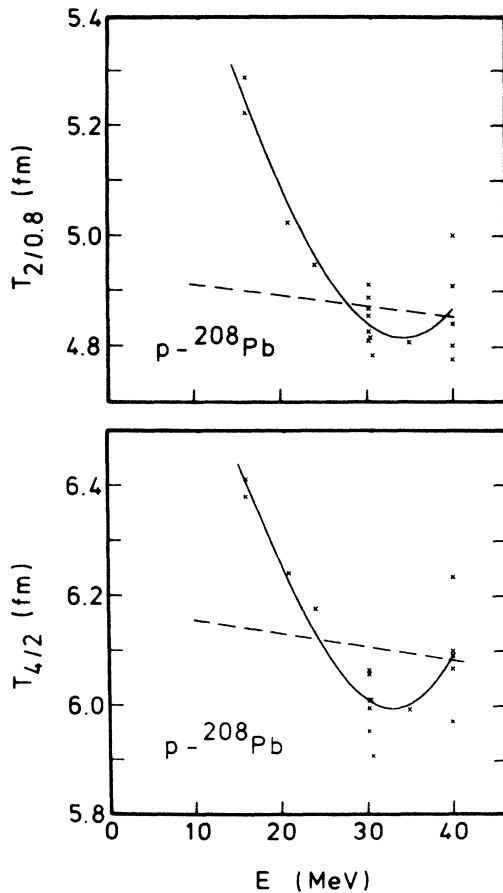


FIG. 4. Energy dependence of the quantities $T_{2/0.8}$ and $T_{4/2}$ associated with the OMP for protons on ^{208}Pb . The crosses represent empirical values. The solid curves are obtained by approximating in Eq. (8) the moments $[r^q]$ and $[r^{q'}]$ by their quadratic approximations [see Eq. (5) and the solid curves in Figs. 1–3]. The dashed lines have been calculated from the nuclear matter approach.

$$\langle r^2 \rangle^{1/2} = T_{4/2} = \{[r^4]/[r^2]\}^{1/2}. \quad (9)$$

The quantities $T_{2/0.8}$ and $T_{4/2}$ in the case of the OMP of protons on ^{208}Pb are represented in Fig. 4. They both present a sizable decrease when E increases from 16 to 30 MeV. It would be of interest to confirm this decrease by performing careful analyses of the experimental cross sections which are available at 17 MeV (Ref. 22) and 26.3 MeV (Ref. 7). We note that experimental data are available below 16 MeV, namely at 8, 9, 10.2, 11, 11.2, 12, 12.8, 12.98, 13, and 14 MeV.⁵ However, these data have been analyzed with OMP's in which the geometrical parameters r_0 and a were fixed *a priori*. This was possible because the calculated cross sections are not very sensitive to the values of r_0 and a for energies located below the top of the Coulomb barrier (≈ 16 MeV for protons on ^{208}Pb). The corresponding OMP's have thus not been retained in the present study. We return to this point in Sec. VII.

In the case of the OMP's of neutrons on ^{208}Pb , the quantities $T_{2/0.8}$ and $T_{4/2}$ are represented in Fig. 5. They both decrease when the energy increases from 4 to 20 MeV. The seven empirical values located between 4 and 7 MeV lie on a horizontal because the corresponding OMP's share the same values of r_0 and a ; they have nevertheless been retained in the present study because it has been

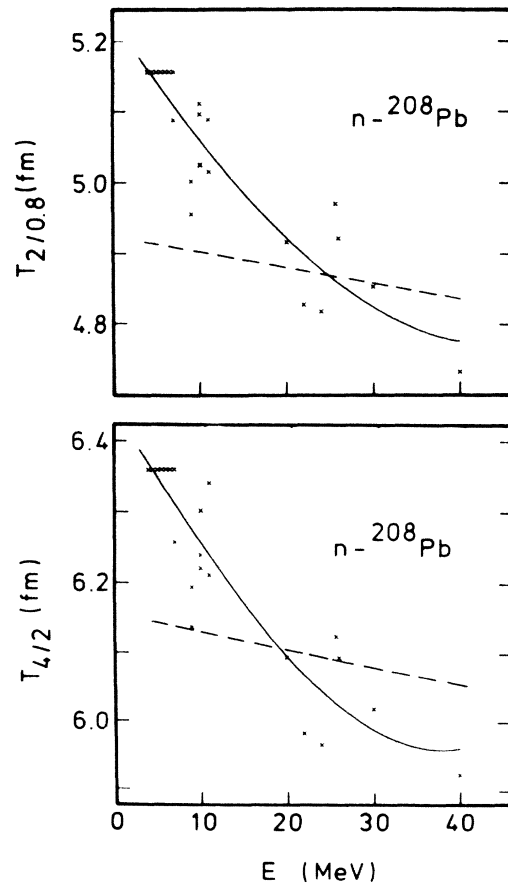


FIG. 5. Same as Fig. 4, in the case of neutrons on ^{208}Pb .

demonstrated in Ref. 2 that in the case of 4–7 MeV neutrons the calculated cross sections are quite sensitive to the values of r_0 and a ; this sensitivity is, however, not sufficient to detect the very small change that r_0 and a may have in the narrow energy domain 4–7 MeV. We note that a decrease of the root mean square radius $T_{4/2}$ with increasing energy also emerges from “model-independent” analyses of n- ^{208}Pb scattering, in which the radial shape of the OMP is parameterized by a Fourier-Bessel sum and is thus not requested to have a Woods-Saxon shape.³

The quantities $T_{2/0.8}$ and $T_{4/2}$ for the system p + ^{20}Ca are represented in Fig. 6. Both quantities appear to increase between 10 and 20 MeV, in contrast to the behavior found in the cases p- ^{208}Pb and n- ^{208}Pb . The empirical data are not sufficient to determine the values of $T_{2/0.8}$ and $T_{4/2}$ in the energy domain 20–40 MeV. Careful phenomenological analyses¹⁷ suggest that the detailed experimental cross sections which are available at 26.3 and 30.3 MeV cannot be accurately fitted if the real part of the OMP is requested to have the Woods-Saxon shape (1): At these energies accurate fits have been obtained only by allowing for oscillations in the radial shape,^{23,24} or by introducing in the OMP a component which depends upon the orbital angular momentum of the projectile, which amounts to a special form of nonlocality.

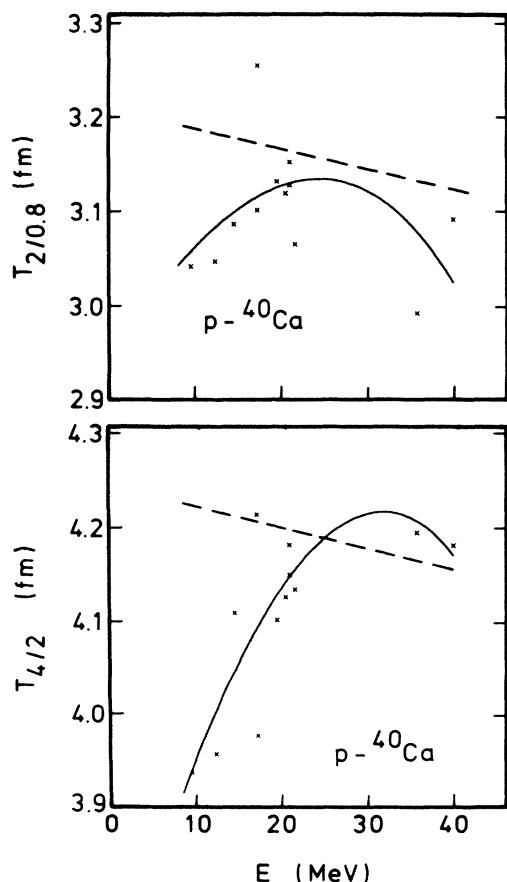


FIG. 6. Same as Fig. 4, in the case of protons on ^{40}Ca .

V. POTENTIAL RADIUS AND SURFACE DIFFUSENESS

If the OMP has a Woods-Saxon shape, the two quantities $T_{2/0.8}$ and $T_{4/2}$ determine the geometrical parameters r_0 and a . Since all the empirical OMP's included in the present compilation have a Woods-Saxon shape, the values of r_0 and a which would be obtained from the empirical values of $T_{2/0.8}$ and $T_{4/2}$ are the same as those determined in the phenomenological analyses. One therefore expects from Figs. 4–6 that the empirical values of r_0 and/or a should display a systematic energy dependence in the energy domains in which both $T_{2/0.8}$ and $T_{4/2}$ are well determined and depend upon energy, namely 16–30 MeV (p- ^{208}Pb), 4–20 MeV (n- ^{208}Pb), and 10–20 MeV (p- ^{40}Ca). This is confirmed in Figs. 7–9. There, the solid curves represent quadratic least squares fits to the empirical values of a and r_0 ; we checked that they are very close to the values of a and r_0 which reproduce the least squares fits to the empirical values of $T_{2/0.8}$ and $T_{4/2}$ (Figs. 4–6).

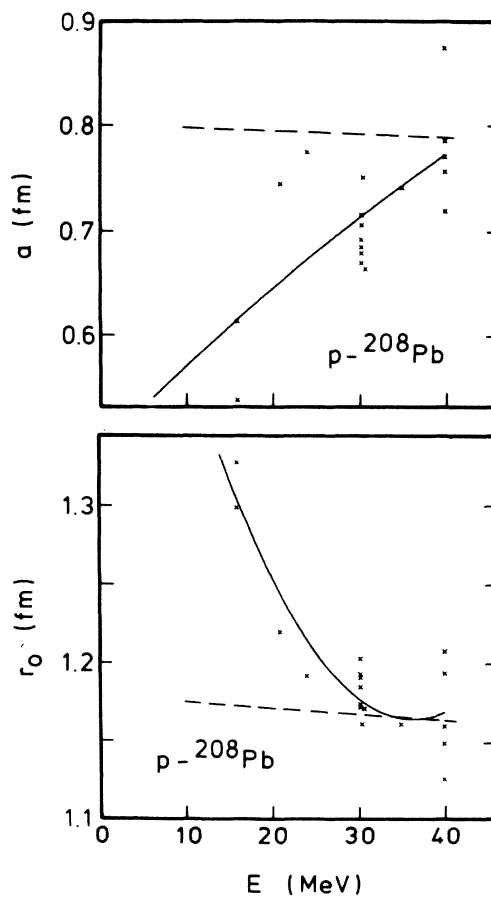


FIG. 7. Energy dependence of the geometrical parameters r_0 and a , in the case of the OMP for protons on ^{208}Pb . The crosses are associated with the empirical OMP's listed in Sec. II. The solid curve represents a least squares fit with a polynomial of second order in E . The long dashes have been calculated from the nuclear matter approach.

In the case $p + {}^{208}\text{Pb}$, the values of r_0 decrease and those of the diffuseness a increase when the bombarding energy increases from 16 to 30 MeV. In the case $n + {}^{208}\text{Pb}$, the values of r_0 also decrease with increasing energy, but those of the diffuseness a are compatible with the constant value 0.705 ± 0.025 fm. In the system $p + {}^{40}\text{Ca}$ the values of r_0 decrease while those of a increase with increasing energy.

VI. NUCLEAR MATTER APPROACH

In the nuclear matter approach of Ref. 4, the OMP is given by the folding approximation,

$$V(r;E) = -(t\sqrt{\pi})^{-3} \int v_E(\rho(r')) \times \exp(-|\mathbf{r}-\mathbf{r}'|^2/t^2) \rho(r') d^3r', \quad (10)$$

where $\rho(r')$ denotes the matter density distribution, while

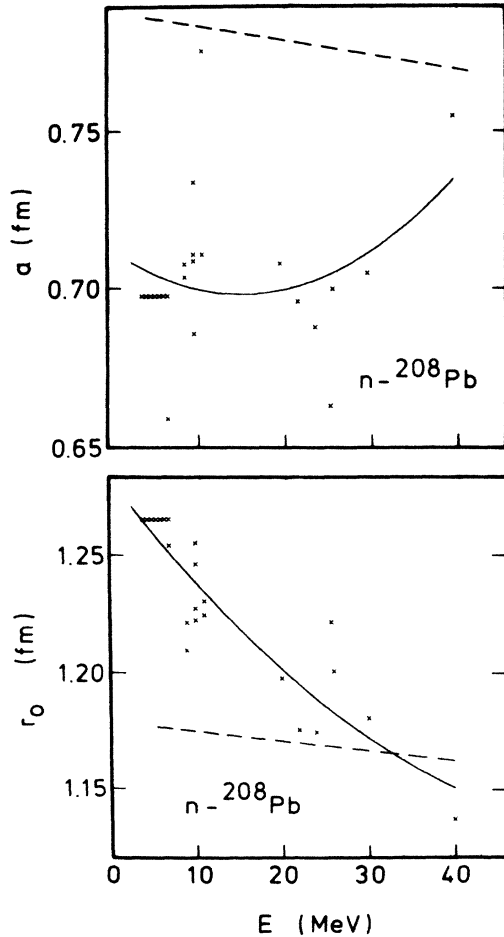


FIG. 8. Same as Fig. 7, for the system $n-{}^{208}\text{Pb}$.

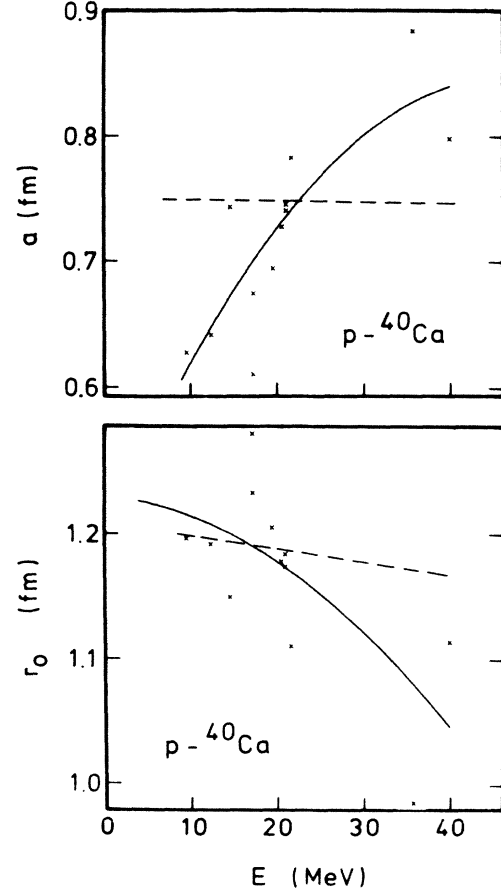


FIG. 9. Same as Fig. 7, for the system $p-{}^{40}\text{Ca}$.

t is an adjustable range parameter and $v_E(\rho)$ an energy- and density-dependent interaction strength. Figure 1 of Ref. 4 shows that the strength $v_E(\rho)$ decreases with increasing ρ and that this density dependence becomes weaker when the energy E increases. The density dependence of $v_E(\rho)$ is responsible for the fact that the half-depth radius R of the calculated OMP, $V(r;E)$, is larger than that of the density distribution $\rho(r)$. Since the density dependence of $v_E(\rho)$ decreases with increasing E , the calculated half-potential radius decreases with increasing E .²⁵ While this trend agrees with the empirical one, we note that the same reasoning indicates that the calculated surface diffuseness increases with decreasing E , which is in contradiction with the empirical trend.

We now show that, in the nuclear matter approach of Ref. 4, the energy dependence of the theoretical values of r_0 and a is, anyhow, practically negligible. We have calculated the values of $V(r;E)$ from the parametric expressions of $v_E(\rho)$ and of $\rho(r)$ given in Ref. 4, and from the choice $t=1.5$ fm for the range parameter. We then computed the radial moments $[r^4]$, $[r^2]$, and $[r^{0.8}]$. One should not expect these calculated moments to be in perfect agreement with the empirical ones. Indeed, the Brueckner-Hartree-Fock approximation in nuclear matter is not exact; moreover, Eq. (10) involves a local density approximation. In order to allow for these inaccuracies, it

is customary (see, e.g., Refs. 26–28) to multiply the calculated potential by a normalization factor λ whose closeness to unity measures the reliability of the nuclear matter approach. Here we took $\lambda=1$ in the cases p-²⁰⁸Pb and p-⁴⁰Ca, and $\lambda=0.97$ in the case n-²⁰⁸Pb. The resulting moments are represented by dashes in Figs. 1–3; their energy dependence is practically linear.

We recall that the nuclear matter approach accounts quite well for the overall energy dependence of $[r^2]$ between 20 and 150 MeV.⁴ Figures 4–6 show that, below 20 MeV, the energy dependence of the calculated moments $[r^q]$ differs from that of the empirical ones, especially for $q=4$. This indicates a failure of the nuclear matter approach at low energy and in the potential surface.

The calculated values of the quantities $T_{2/0.8}$ and $T_{4/2}$ are represented by the dashes in Figs. 4–6. Note that they are independent of the normalization factor λ . Their energy dependence is much weaker than the one displayed by the empirical values.

From the calculated $T_{2/0.8}$ and $T_{4/2}$ one can compute the geometrical parameters r_0 and a if one assumes that the calculated OMP has a Woods-Saxon shape. The results are represented by the dashed lines in Figs. 7–9. In keeping with the previous reasoning the calculated r_0 and a decrease with increasing E . We note, however, that the decrease of the calculated r_0 is much weaker than that of the empirical r_0 . Moreover, we observe that the calculated diffuseness decreases with increasing E while the empirical one increases.

It therefore appears that the nuclear matter approach of Ref. 4 does not explain the observed energy dependence of the radial shape at low energy. It is not excluded that a modified nuclear matter approach based on a different type of local density approximation (see, e.g., Refs. 29 and 30) would modify the calculated energy dependence of the radial shape. This is difficult to evaluate because these approaches yield nonlocal OMP's. The local equivalent potential considered in Ref. 25 depends upon the orbital angular momentum l ; moreover it does not have a Woods-Saxon shape for fixed l , so that the quantities r_0 and a do not have a well-defined meaning.

Finally, we note that the local equivalent potential of the Hartree-Fock field associated with a Skyrme-type effective interaction also has an energy-dependent radial shape, because of the momentum dependence of the effective interaction. This can be seen from the expressions given in Ref. 31. We have checked that the corresponding energy dependence of $T_{2/0.8}$ and of $T_{4/2}$ is very weak and that, moreover, these calculated quantities increase with increasing energy while the empirical quantities decrease.

VII. SUMMARY AND DISCUSSION

Figures 1–3 show that the radial moments [Eq. (3)] $[r^{0.8}]$, $[r^2]$, and $[r^4]$ of the empirical OMP are fairly well determined in the energy domains $16 \leq E \leq 40$ MeV (p-²⁰⁸Pb), $4 \leq E \leq 40$ MeV (n-²⁰⁸Pb), and $10 \leq E \leq 40$ MeV (p-⁴⁰Ca), with the restriction that in the latter case the standard Woods-Saxon parametrization does not yield accurate fits to the experimental cross sections in the inter-

val $22 < E < 35$ MeV.

Figures 4–6 show that the ratios $[r^2]/[r^{0.8}]$ and $[r^4]/[r^2]$ vary with energy in the domains $16 < E < 30$ MeV (p-²⁰⁸Pb), $4 < E < 25$ MeV (n-²⁰⁸Pb), and $10 < E < 20$ MeV (p-⁴⁰Ca). This energy dependence indicates that, in these domains, the radial shape of the OMP depends upon energy. In the case n-²⁰⁸Pb this confirms conclusions recently drawn in Refs. 1–3.

In the three systems, the potential radius $R=r_0A^{1/3}$ decreases with increasing energy for $E < 25$ MeV. The surface diffuseness increases with E in the cases p-²⁰⁸Pb and p-⁴⁰Ca and is essentially constant in the case n-²⁰⁸Pb. It appears questionable that the energy dependence of the radial shape is mainly due to the energy dependence of the effective interaction as had been proposed in Ref. 25. Indeed, while theoretical calculations carried out in the framework of the nuclear matter approach predict an energy dependence of the radial shape, this dependence is much weaker than the one observed empirically. This is shown by the dashed lines in Figs. 4–9.

We believe that it is more likely that the energy dependence of the radial shape at low energy is mainly due to the contribution to the OMP of the coupling between the elastic channel and the inelastic channels associated with surface vibrations. Schematic calculations³² indicate that the potential radius increases when the energy decreases below 20 MeV. It is predicted to decrease at very low energy.³² More detailed calculations are in progress, for the three systems considered in the present paper. It would be of interest to investigate whether the decrease predicted at very low energy is compatible with the experimental data. We note that in the case p-²⁰⁸Pb accurate fits have been obtained in the domain $8 < E < 14$ MeV with the energy-independent geometrical parameters $r_0=1.25$ fm and $a=0.65$ fm (Ref. 33) ($E=8, 9, 10.2, 11.2, 12, 12.8$, and 14 MeV), or $r_0=1.17$ fm and $a=0.72$ fm (Ref. 34) ($E=11$ and 13 MeV). These two sets suggest a turnover of the trend found at higher energies (Fig. 7), in qualitative agreement with the effect expected from the coupling to surface vibrations.

Most available phenomenological optical-model analyses adopt the assumption that $V(r;E)$ has a Woods-Saxon shape. More detailed information on the radial shape can hardly be expected since accurate fits to the experimental cross sections are obtained within this assumption. It is of interest to note that “model-independent Fourier-Bessel” analyses of the n-²⁰⁸Pb scattering cross sections have been performed;³ they confirm that the potential root mean square radius decreases with increasing energy in the domain $4 < E < 20$ MeV.

In conclusion, we have shown that for the systems p-²⁰⁸Pb, n-²⁰⁸Pb, and p-⁴⁰Ca the radial shape of the real part of the empirical OMP rapidly varies with energy in the domain $10 < E < 20$ MeV. We recommend that the experimental data which are available at $E < 20$ MeV, and for which very good fits have not yet been obtained, be reanalyzed. The empirical evidence is sufficiently pronounced to call for a detailed theoretical understanding. The nuclear matter approach does not explain the observed energy dependence. A likely origin lies in the polarization corrections due to the excitation of the surface

vibrations of the target nucleus. The available calculations are somewhat schematic.³² They predict that the potential radius increases with energy at negative energy, becomes constant at very low positive energies, and decreases in the domain $10 < E < 20$ MeV. The predictions

of this model should be refined and confronted with the empirical behavior exhibited in the present paper.

We are very grateful to M. Jaminon for having calculated the dashed lines in Figs. 1–6.

-
- ¹R. W. Finlay, J. R. M. Annand, T. S. Cheema, J. Rapaport, and F. S. Dietrich, *Phys. Rev. C* **30**, 796 (1984).
²J. R. M. Annand, R. W. Finlay, and F. S. Dietrich, *Nucl. Phys.* **A443**, 249 (1985).
³R. W. Finlay and J. S. Petler, in *Use of the Optical Model for the Calculation of Neutron Cross Sections below 20 MeV* (OECD, Paris, 1986), pp. 43–52.
⁴J.-P. Jeukenne, A. Lejeune, and C. Mahaux, *Phys. Rev. C* **16**, 80 (1977).
⁵C. M. Perey and F. G. Perey, *At. Data Nucl. Data Tables* **17**, 1 (1976).
⁶W. Makofske, G. W. Greenlees, H. S. Liers, and G. J. Pyle, *Phys. Rev. C* **5**, 780 (1972).
⁷W. T. H. Van Oers, Huang Haw, N. E. Davison, A. Ingemarsson, B. Fagerström, and G. Tibell, *Phys. Rev. C* **10**, 307 (1974).
⁸R. C. Barrett, A. D. Hill, and P. E. Hodgson, *Nucl. Phys.* **62**, 133 (1965).
⁹G. R. Satchler, *Nucl. Phys.* **A92**, 273 (1967).
¹⁰G. W. Greenlees, V. Hnidzo, O. Karban, J. Lowe, and W. Makofske, *Phys. Rev. C* **2**, 1063 (1970).
¹¹F. G. Perey, in *Polarization Phenomena in Nuclear Reactions*, edited by H. H. Barschall and W. Haeberli (University of Wisconsin, Madison, 1971), pp. 131.
¹²M. P. Fricke and G. R. Satchler, *Phys. Rev.* **139**, B567 (1965).
¹³M. P. Fricke, E. E. Gross, B. J. Morton, and A. Zucker, *Phys. Rev.* **156**, 1207 (1967).
¹⁴J. Rapaport, T. S. Cheema, D. E. Bainum, R. W. Finlay, and J. D. Carlson, *Nucl. Phys.* **A296**, 95 (1978).
¹⁵J. P. Delaroche, C. E. Floyd, P. P. Guss, R. C. Byrd, K. Murphy, G. Tungate, and R. L. Walter, *Phys. Rev. C* **28**, 1410 (1983).
¹⁶W. T. H. Van Oers, *Phys. Rev. C* **3**, 1550 (1971).
¹⁷A. M. Kobos and R. S. Mackintosh, *J. Phys. G* **5**, 97 (1979).
¹⁸K. H. Bray, K. S. Jayaraman, G. A. Moss, W. T. H. Van Oers, D. O. Wells, and Y. I. Wu, *Nucl. Phys.* **A167**, 57 (1971).
¹⁹C. Mahaux and R. Sartor, *Nucl. Phys.* **A458**, 25 (1986).
²⁰J. Rapaport, *Phys. Rep.* **87**, 25 (1982).
²¹C. Mahaux and H. Ngô, *Phys. Lett.* **126B**, 1 (1983).
²²G. Schrank and R. E. Pollock, *Phys. Rev.* **132**, 2200 (1963).
²³A. M. Kobos and R. S. Mackintosh, *Ann. Phys. (N.Y.)* **123**, 296 (1979).
²⁴A. A. Ioannides and A. M. Kobos, *Nucl. Phys.* **A438**, 354 (1985).
²⁵M. Kohno, D. W. L. Sprung, S. Nagata, and N. Yamaguchi, *Phys. Lett.* **137B**, 10 (1984).
²⁶S. Mellema, R. W. Finlay, F. S. Dietrich, and F. Petrovich, *Phys. Rev. C* **28**, 2267 (1983).
²⁷L. F. Hansen, F. S. Dietrich, B. A. Pohl, C. H. Poppe, and C. Wong, *Phys. Rev. C* **31**, 111 (1985).
²⁸J. S. Petler, M. S. Islam, R. W. Finlay, and F. S. Dietrich, *Phys. Rev. C* **32**, 673 (1985).
²⁹F. A. Brieva and J. R. Rook, *Nucl. Phys.* **A291**, 317 (1977).
³⁰N. Yamaguchi, S. Nagata, and T. Matsuda, *Prog. Theor. Phys.* **70**, 459 (1983).
³¹C. B. Dover and Nguyen Van Giai, *Nucl. Phys.* **A190**, 373 (1972).
³²C. Mahaux and H. Ngô, *Nucl. Phys.* **A378**, 205 (1982).
³³T. Mo and R. H. Davis, *Phys. Rev. C* **6**, 231 (1972).
³⁴J. S. Eck and W. J. Thomson, *Nucl. Phys.* **A237**, 83 (1975).